

# An atomic frequency comb memory in rare-earth doped thin-film lithium niobate

Subhajit Dutta<sup>1</sup>, Yuqi Zhao<sup>1</sup>, Uday Saha<sup>1</sup>, Demitry Farfurnik<sup>1</sup>, Elizabeth A. Goldschmidt<sup>2,3</sup>, Edo Waks<sup>1\*</sup>

<sup>1</sup>*Department of Electrical and Computer Engineering, Institute for Research in Electronics and Applied Physics, and Joint Quantum Institute, University of Maryland, College Park, MD 20742, USA.*

<sup>2</sup>*Department of Physics, University of Illinois at Urbana-Champaign, Urbana, IL 61801*

<sup>3</sup>*US Army Research Laboratory, Adelphi, MD 20783*

*\*edowaks@umd.edu*

Atomic frequency combs coherently store optical signals, a key building block for optical quantum computers<sup>1</sup> and quantum networks<sup>2</sup>. Integrating an atomic frequency comb memory into a compact and chip-integrated device is essential to achieve scalable quantum technology. But the majority of such memories have been realized using bulk systems or waveguides with large cross-sections that are difficult to integrate into compact chips<sup>3-5</sup>, or using fabrication techniques that are not easily adaptable to wafer scale processing<sup>6</sup>. Here we demonstrate a compact chip-integrated atomic frequency comb in thin-film lithium niobate. We utilize rare-earth doped thin-film lithium niobate<sup>7,8</sup> to demonstrate both coherent control of the atomic ensemble and optical storage using an atomic frequency comb. Our optical memory exhibits a broad storage spectrum exceeding 100 MHz, and optical storage time of over 250 ns. The enhanced optical confinement in our device structure enables coherent rotations on the ions with three orders of magnitude less optical power as compared to previous results in large waveguides. These compact atomic frequency comb memories pave the way towards scalable, highly efficient, electro-optically tunable quantum photonic systems where one can store and manipulate light on chip with high bandwidth and low powers<sup>3</sup>.

Lithium niobate is an ideal photonic platform for developing integrated optical memories based on rare earth ions<sup>7,9-13</sup>. Lithium niobate exhibits a wide transparency window, ranging from the ultraviolet to the telecommunications band, and can be integrated with a range of rare-earth ion species (e.g., praseodymium, thulium, erbium, etc.) that are optically active over this entire wavelength range<sup>11,14</sup>. Rare-earth-doped ion diffused waveguides patterned in bulk lithium niobate have been previously used to demonstrate optical quantum memory<sup>3,15,16</sup>. However, these devices have a large mode cross section resulting in low optical intensities, necessitating high optical

powers for coherent control and storage using atomic frequency combs. Thin-film lithium niobate provides a more compact device structure that is compatible with wafer scale fabrication<sup>17</sup>. Progress in the processing and fabrication of this material achieved extremely low waveguide loss<sup>18</sup> and high-speed electro-optic modulation<sup>19</sup>. Recent efforts to incorporate thulium into thin film lithium niobate have shown bulk-like optical properties which are promising for engineering a photonic memory<sup>7,8,20</sup>. But atomic frequency comb memories with these materials have yet to be realized.

In this letter we report an atomic frequency comb memory in thulium-doped thin-film lithium niobate waveguides. We pattern an atomic frequency comb<sup>1,3</sup> on the absorption spectrum of the thulium ion ensemble by spectral hole-burning and achieve optical storage times exceeding 200 ns<sup>1,3</sup>. Through a photon echo measurement we observe a coherence time of  $700 \pm 96$  ns, matching values of the bulk materials. Due to tight confinement of the waveguide, the ions in the thin film exhibit a three orders of magnitude enhancement in Rabi frequency as compared to ion-diffused waveguides<sup>16</sup>. Such integrated optical memories could serve as fundamental components for high bandwidth quantum information processors on-a-chip<sup>21,22</sup>.

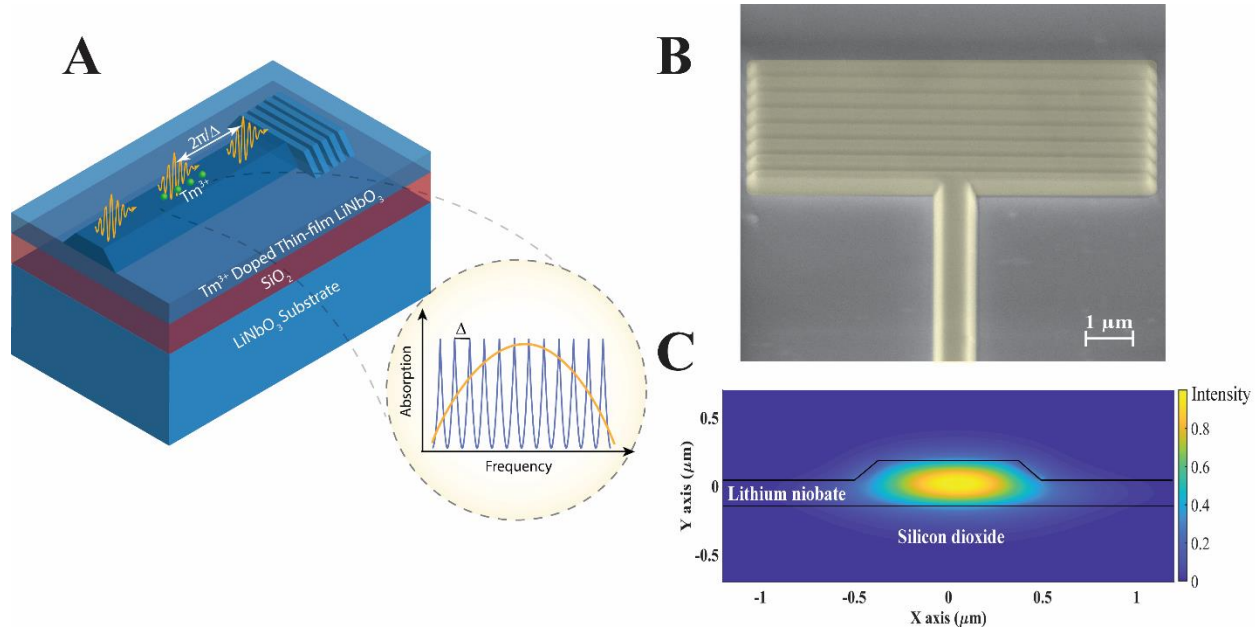


Figure 1. (A) A schematic illustration of the thulium-doped thin film lithium niobate nanophotonic waveguide. (B) Scanning electron microscopy image of the waveguide with grating couplers. (C) Finite difference time domain simulation showing the electric field in the waveguide.

Figure 1A shows a schematic of the device structure, which consists of a 0.8 mm long ridge waveguide patterned in thin-film lithium niobate. The thin-film lithium niobate is doped with thulium ions at a density of 0.1%. The thulium ions are an on-chip absorber that stores and re-emits light creating an optical memory. Figure 1(B) shows a scanning electron microscope image of a fabricated waveguide with grating coupler to couple light in and out of the chip. The fabrication details were reported in earlier work<sup>7</sup> and are also provided in supplementary section

S1. Figure 1(C) shows the calculated cross-sectional mode profile of the simulated TE mode in the thin film waveguide. The optical mode exhibits a transverse area of (176 nm X 400 nm)  $0.07 \mu\text{m}^2$ , which is three orders of magnitude smaller than ion-diffused waveguides<sup>16</sup>. This leads to strong light confinement and high field intensities within the waveguide.

We first characterize the coherence time of the atomic ensemble, which puts a fundamental limit on the storage time of the medium. We perform this measurement using a photon-echo pulse sequence, shown in Fig. 2A. The pulse sequence, uses two laser pulses to coherently rotate the atomic population. The first laser pulse has a pulse area corresponding to a  $\pi/2$  pulse, which coherently rotates the population to a superposition of the ground and excited state. The second pulse, delayed by time  $\tau$ , has twice the pulse duration resulting in a  $\pi$ -pulse that rephases the atomic population. This rephasing results in a photon echo delayed by a time  $\tau$  relative to the rephasing pulse. By measuring the strength of the photon echo as a function of  $\tau$  we can determine the coherence time of the rare-earth ensemble.

We implement the rotation pulses using a resonant laser pulse shaped from a continuous wave laser (see supplementary section S2 for additional details). To determine the pulse intensities that achieve the  $\pi$  and  $\pi/2$  condition, we plot the power of the output photon echo as a function of rephasing pulse duration, keeping the first pulse duration fixed. Figure 2B shows the measured results which exhibit Rabi oscillation with an optimal  $\pi$  pulse duration of 70 ns. From the pulse width of the  $\pi$  pulse, we determine that the Rabi frequency of the dipole transition is 44.9 MHz ( $\pi/t_2$ ) for a driving power of 1  $\mu\text{W}$  in the waveguide (see supplementary section S3 for additional details). This power is three orders of magnitude smaller than the power required to achieve the same Rabi frequency in ion diffused waveguides<sup>16</sup>.

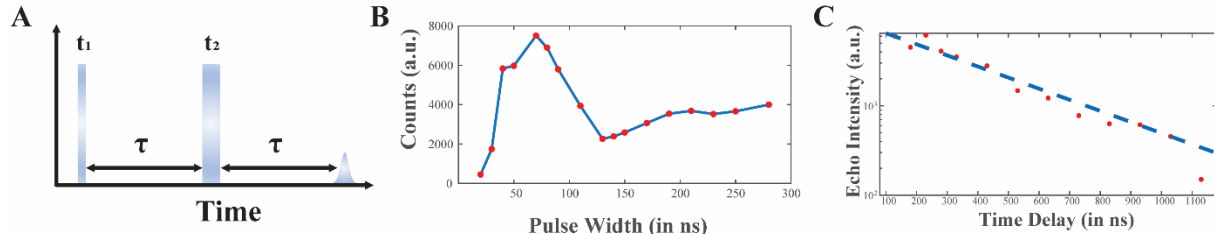


Figure 2. (A) The schematic shows the pulse sequence for performing two photon echoes. (B) The figure demonstrates an oscillating echo intensity with an increasing width of the rephasing pulse. The periodic signal reveals the ensemble averaged Rabi frequency of the coupled ions. (C) The photon echo intensity decays with increasing delay time between the two pulses. A single exponential fit reveals the characteristic decay time or coherence time of the ions in the thin film

Figure 2C shows the photon echo amplitude as a function of the delay  $\tau$ . The echo decays with an exponential time constant of  $350 \pm 48$  ns. From this measurement we determine the coherence time  $T_2 = 2\tau$  to be  $700 \pm 96$  ns, which corresponds to a homogeneous linewidth of 450 kHz. This linewidth is comparable to previous measurements for thulium ions in bulk lithium niobate at 4

K<sup>9</sup>, indicating that thin-film processing does not significantly degrade the coherence properties of the rare-earth ions.

To realize an atomic frequency comb memory, we implement the pulse sequence illustrated in Figure 3A composed of a periodic pulse train. The pulse train burns a series of spectral holes at fixed frequency intervals, thereby creating an atomic frequency comb<sup>1,3</sup>. When a pulse enters the prepared atomic ensemble, it excites the individual comb teeth which rapidly dephase, and then rephase at a time  $2\pi/\Delta$  and re-emit the photon. To burn the comb, we send a pulse train of 150 pulses with pulse duration 10 ns and variable period  $T = 2\pi/\Delta$  that sets the storage time. We set the peak power of the comb sequence at 0.5  $\mu$ W in the waveguide (see supplementary section S3 for a detailed discussion).

Figure 3(B) shows the absorption spectrum of the atomic ensemble after the comb burning pulse sequence using a burn pulse sequence with period of  $T = 130$  ns. We measure this absorption spectrum by sweeping the frequency of a weak probe, which is attenuated by three orders of magnitude relative to burn pulse. We inject the probe pulse through the ion ensemble and measure the light at the output grating. The absorption spectrum features a series of absorption lines corresponding to the different comb teeth. The combs spacing is 6.3 MHz, as expected for the selected pulse periodicity (see supplementary section S4 for a detailed discussion). The measured atomic frequency comb has an optical depth contrast of 0.23. The average full-width half-maximum linewidth is 2.9 MHz, corresponding to a comb finesse of 2.17. Also, the rise in the intensity over the different comb teeth is due to the spectrum of the input pulse, which is induced by the acousto-optical modulator bandwidth of 50 MHz.

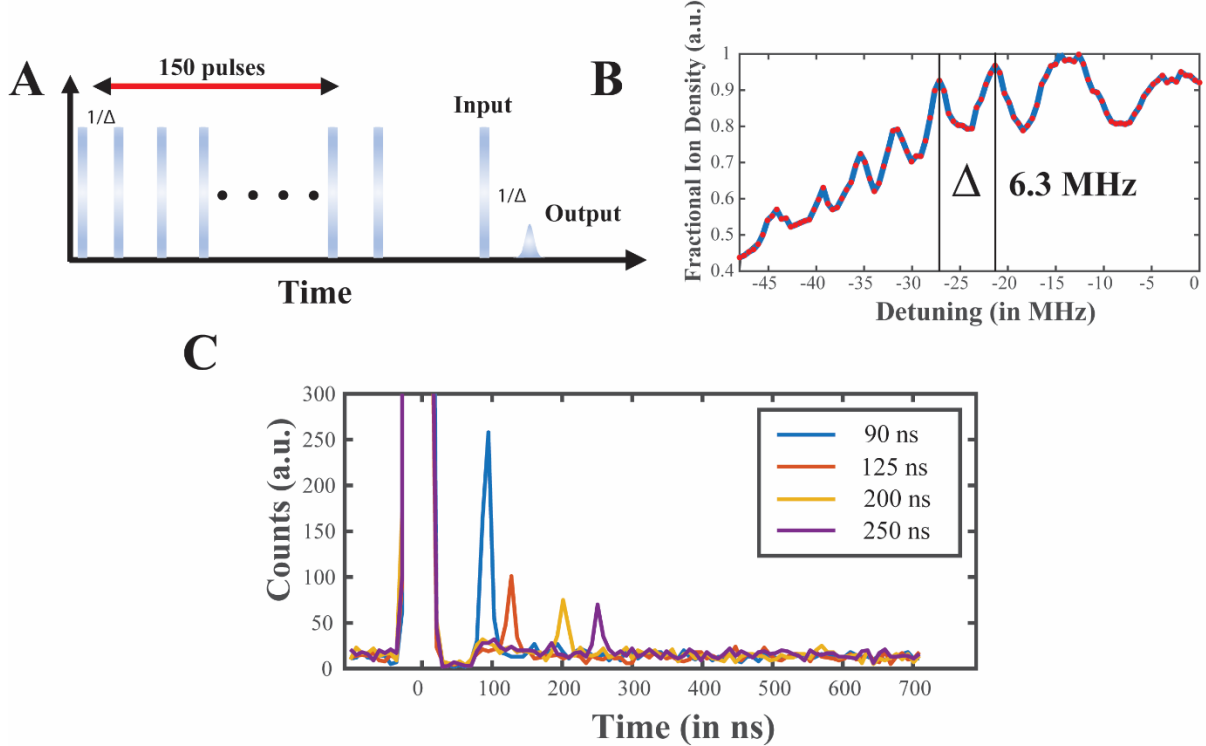


Figure 3. (A) The schematic shows the experimental pulse sequence for achieving an atomic frequency comb. (B) The broadband frequency sweep maps the structure of the atomic frequency comb. (C) Photon storage for different storage times in the integrated memory device.

To store light in the atomic frequency comb memory, we inject a 10 ns optical pulse at 794.2 nm, the center frequency of the atomic frequency comb. Figure 3C shows that waveguide output for several different frequency combs corresponding to storage times ranging from 90 ns to 250 ns. Each comb results in an output pulse that is delayed by the correct time programmed into the frequency comb memory. We calculate the storage efficiency of the comb, defined as the ratio of the input and output pulse energies to be 0.14% for a 90 ns storage time (see supplementary section S5). This storage is primarily limited by the small optical depth contrast that we can achieve. The storage efficiency decreases as we increase the storage time of the system. For a storage time of 130 ns the efficiency decreases to 0.09%, while at 250 ns it further reduces to 0.03%. We note that the storage efficiency does not exhibit single exponential decay, as would be expected if pure dephasing process of the thulium transition was dominating the dependence on storage time. We attribute this non-exponential decay to the fact that the finesse of the comb teeth varies significantly with increasing storage time due to the reduced free spectral range bringing the comb teeth closer.

In conclusion, we demonstrated an atomic frequency comb memory in thulium-doped thin film lithium niobate. The tight confinement of the thin-film lithium niobate waveguide led to a three orders of magnitude improvement in the Rabi frequency and we observed no degradation of

the coherence properties of the thulium dopants compared to bulk materials. We can further improve the storage efficiency by increasing the optical depth of the atomic frequency comb by burning the frequency comb in the presence of a magnetic field and using the Zeeman split levels to pattern the absorption spectrum<sup>3</sup>. As a further extension, we can take advantage of the thin film platform and design impedance matched cavities<sup>18,23,24</sup> as a pathway to achieving a unit efficiency optical memory on chip<sup>25</sup>. Thin film lithium niobate offers a rich diversity as a photonic material providing strong optical nonlinearity<sup>19</sup>. The ability to integrate active modulation on chip would lead to an electro-optically tunable<sup>26</sup> integrated photonic memory. Such a versatile platform is therefore a critical step which paves way for scalable, highly efficient, electro-optically tunable quantum photonic systems where one can store and manipulate light on chip with high bandwidth and low powers.

1. Afzelius, M., Simon, C., de Riedmatten, H. & Gisin, N. Multimode quantum memory based on atomic frequency combs. *Phys. Rev. A* **79**, 52329 (2009).
2. Kimble, H. J. The quantum internet. *Nature* **453**, 1023–1030 (2008).
3. Saglamyurek, E. *et al.* Broadband waveguide quantum memory for entangled photons. doi:10.1038/nature09719.
4. Davidson, J. H., Lefebvre, P., Zhang, J., Oblak, D. & Tittel, W. Improved light-matter interaction for storage of quantum states of light in a thulium-doped crystal cavity. *Phys. Rev. A* **101**, 42333 (2020).
5. Corrielli, G., Seri, A., Mazzera, M., Osellame, R. & de Riedmatten, H. Integrated Optical Memory Based on Laser-Written Waveguides. *Phys. Rev. Appl.* **5**, 54013 (2016).
6. Zhong, T. *et al.* Nanophotonic rare-earth quantum memory with optically controlled retrieval. *Science* (80-. ). (2017) doi:10.1126/science.aan5959.
7. Dutta, S., Goldschmidt, E. A., Barik, S., Saha, U. & Waks, E. Integrated Photonic Platform for Rare-Earth Ions in Thin Film Lithium Niobate. *Nano Lett.* **20**, 741–747 (2020).
8. Jiang, X., Pak, D., Nandi, A., Xuan, Y. & Hosseini, M. Rare earth-implanted lithium niobate: Properties and on-chip integration. *Appl. Phys. Lett.* **115**, 71104 (2019).
9. Sun, Y., Thiel, C. W. & Cone, R. L. Optical decoherence and energy level structure of 0.1%Tm<sup>3+</sup>:LiNbO<sub>3</sub>. *Phys. Rev. B* **85**, 165106 (2012).
10. Thiel, C. W., Sun, Y., Böttger, T., Babbitt, W. R. & Cone, R. L. Optical decoherence and persistent spectral hole burning in Tm<sub>3</sub>:LiNbO<sub>3</sub>. in *Journal of Luminescence* (2010). doi:10.1016/j.jlumin.2009.12.019.
11. Thiel, C. W., Sun, Y., Macfarlane, R. M., Böttger, T. & Cone, R. L. Rare-earth-doped LiNbO<sub>3</sub> and KTiOPO<sub>4</sub> (KTP) for waveguide quantum memories. *J. Phys. B At. Mol. Opt. Phys.* (2012) doi:10.1088/0953-4075/45/12/124013.
12. Thiel, C. W., Böttger, T. & Cone, R. L. Rare-earth-doped materials for applications in

quantum information storage and signal processing. *J. Lumin.* **131**, 353–361 (2011).

- 13. Thiel, C. W. & Böttger, T. Rare-Earth-Doped Materials with Application to Optical Signal Processing , Quantum Information Science , and Medical Imaging Technology. (2012) doi:10.1117/12.909154.
- 14. Boes, A., Corcoran, B., Chang, L., Bowers, J. & Mitchell, A. Status and Potential of Lithium Niobate on Insulator (LNOI) for Photonic Integrated Circuits. *Laser Photonics Rev.* **12**, 1–19 (2018).
- 15. Sinclair, N. *et al.* Spectroscopic investigations of a Ti: Tm LiNbO<sub>3</sub> waveguide for photon-echo quantum memory. in *Journal of Luminescence* (2010). doi:10.1016/j.jlumin.2009.12.022.
- 16. Sinclair, N., Oblak, D., Thiel, C. W., Cone, R. L. & Tittel, W. Properties of a Rare-Earth-Ion-Doped Waveguide at Sub-Kelvin Temperatures for Quantum Signal Processing. *Phys. Rev. Lett.* (2017) doi:10.1103/PhysRevLett.118.100504.
- 17. Luke, K. *et al.* Wafer-scale low-loss lithium niobate photonic integrated circuits. *Opt. Express* **28**, 24452–24458 (2020).
- 18. Zhang, M., Wang, C., Cheng, R., Shams-Ansari, A. & Loncar, M. Monolithic Ultrahigh-Q Lithium Niobate Microring Resonator. (2017) doi:10.1364/OPTICA.4.001536.
- 19. Wang, C., Zhang, M., Stern, B., Lipson, M. & Loncar, M. Nanophotonic Lithium Niobate Electro-optic Modulators. (2017) doi:10.1364/OE.26.001547.
- 20. Wang, S. *et al.* Incorporation of erbium ions into thin-film lithium niobate integrated photonics. *Appl. Phys. Lett.* **116**, 151103 (2020).
- 21. Heshami, K. *et al.* Quantum memories: emerging applications and recent advances. *J. Mod. Opt.* **63**, 2005–2028 (2016).
- 22. Zhong, T. & Goldner, P. Review article Emerging rare-earth doped material platforms for quantum nanophotonics. (2019).
- 23. Li, M., Liang, H., Luo, R., He, Y. & Lin, Q. High-Q 2D Lithium Niobate Photonic Crystal Slab Nanoresonators. **1800228**, 1–8 (2019).
- 24. Liang, H., Luo, R., He, Y., Jiang, H. & Lin, Q. High-quality lithium niobate photonic crystal nanocavities. (2017) doi:10.1364/OPTICA.4.001251.
- 25. Afzelius, M. & Simon, C. Impedance-matched cavity quantum memory. *Phys. Rev. A - At. Mol. Opt. Phys.* **82**, 1–4 (2010).
- 26. Fossati, A. *et al.* A frequency-multiplexed coherent electro-optic memory in rare earth doped nanoparticles. *arXiv* (2020).

## Supplementary Information

### **S1. Fabrication**

We begin with a bulk X-cut lithium niobate substrate doped with 0.1% thulium. Using a commercial smart-cut process (NANOLN), we fabricate a 300 nm layer of doped single crystal lithium niobate wafer bonded to a 2  $\mu$ m thick layer of silicon dioxide grown on undoped bulk lithium niobate as the substrate material. We etch waveguides into the doped thin film using a home developed two-layer electron beam lithography and dry etching process.

### **S2. Experimental Setup**

To perform the measurements, we use two fiber coupled acousto-optic modulators (Brimrose Corp.) to carve out pulses at two independent frequencies,  $f_0$  and  $f_1$ , from the single frequency input laser (M2 Solistis). We can switch the modulators by means of an RF switch (Mini circuits)

and control pulses generated by an arbitrary waveform generator. We drive the AOMs using a pair of Voltage Controlled Oscillators which can be tuned to independently control the output frequencies  $f_0$  and  $f_1$ .

### S3. Calibrating Power in the Waveguide

In order to calibrate the power in the waveguide, we measure the end-to-end power transmission through the setup and the device under test. We measure the input power right before the objective lens we use for focusing on the sample grating couplers and measure the output power scattered from the output grating into a single mode fiber. We assume that the in-coupling and out-coupling efficiencies are equal and we have negligible waveguide loss for sub mm long waveguides. Using such a procedure we extract the input and output coupling efficiency as 0.1% each. In this way we have a good order of magnitude estimate of the power coupled into the waveguide.

### S4. Atomic Frequency Comb Preparation

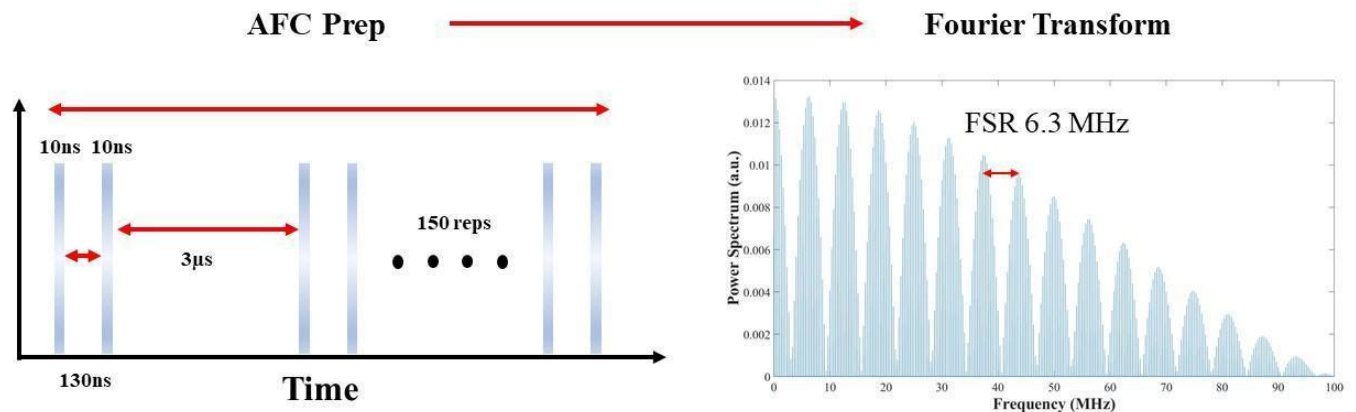


Figure S3. The schematic on the left shows a time domain representation of the pulse sequence for preparing an atomic frequency comb. The figure on the right demonstrates a Fourier transform of the same pulse sequence representing a frequency comb in the Fourier space.

To prepare the atomic frequency comb, we send a series of 10 ns long pulse pairs separated by the programmable storage time (130 ns in Fig S3). The wait time between the pulse pairs is 3  $\mu$ s, which is long compared to coherence time of the ions. We use a series of 150 repetitions to burn a series of spectral holes. The Fourier transform of this pulse sequence consist of a series of frequency peaks separated by 6.3 MHz. This results in a spectral hole every 6.3 MHz which matches well with the experimentally observed free spectral range.

## **S5. Calculating AFC storage efficiency**

The AFC storage efficiency is defined as the ratio of the integrated counts in the output echo pulse and the integrated counts in the input pulse that is stored.